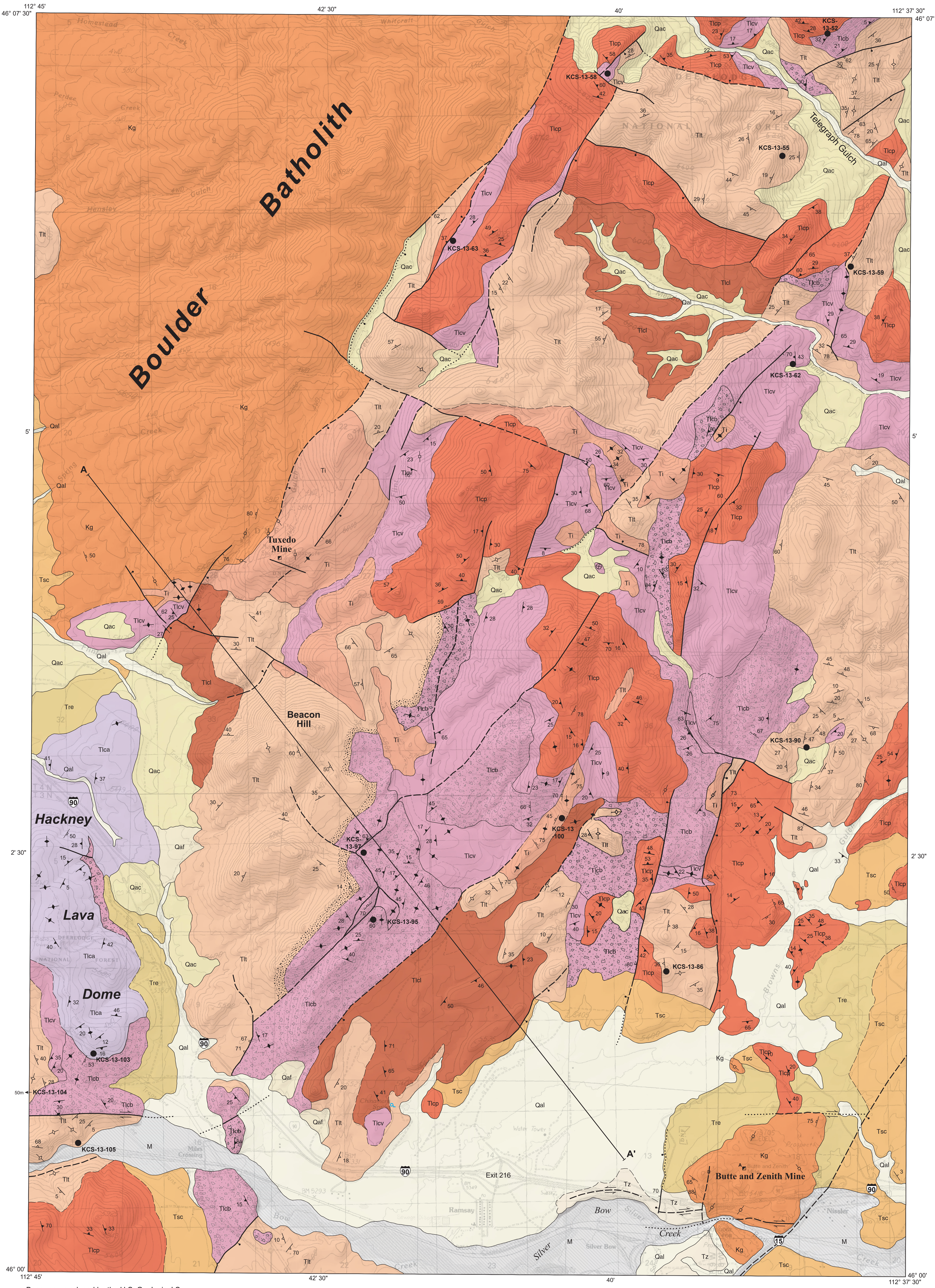

Base map produced by the U.S. Geological Survey
Control by: USGS, NOS/NOAA and USFS
Compiled from aerial photographs taken 1954–1955
Limited revision from aerial photographs taken 1986
Field checked: 1987 Map edited: 1989
Projection: Lambert Conformal Conic
Grid:1000 meter Universal Transverse Mercator Zone 12
UTM grid declination: 1° 13' West
1989 Magnetic North Declination: 16° 30' East
Vertical Datum: National Geodetic Vertical Datum of 1929
Horizontal Datum: 1927 North American Datum

SCALE 1:24,000
CONTOUR INTERVAL 40 FEET
NATIONAL GEODETIC VERTICAL DATUM OF 1929

Maps may be obtained from:
Publications Office
Montana Bureau of Mines and Geology
1300 West Park Street
Butte, Montana 59701-8997
Phone: (406) 496-4174
http://mbmg.mtech.edu

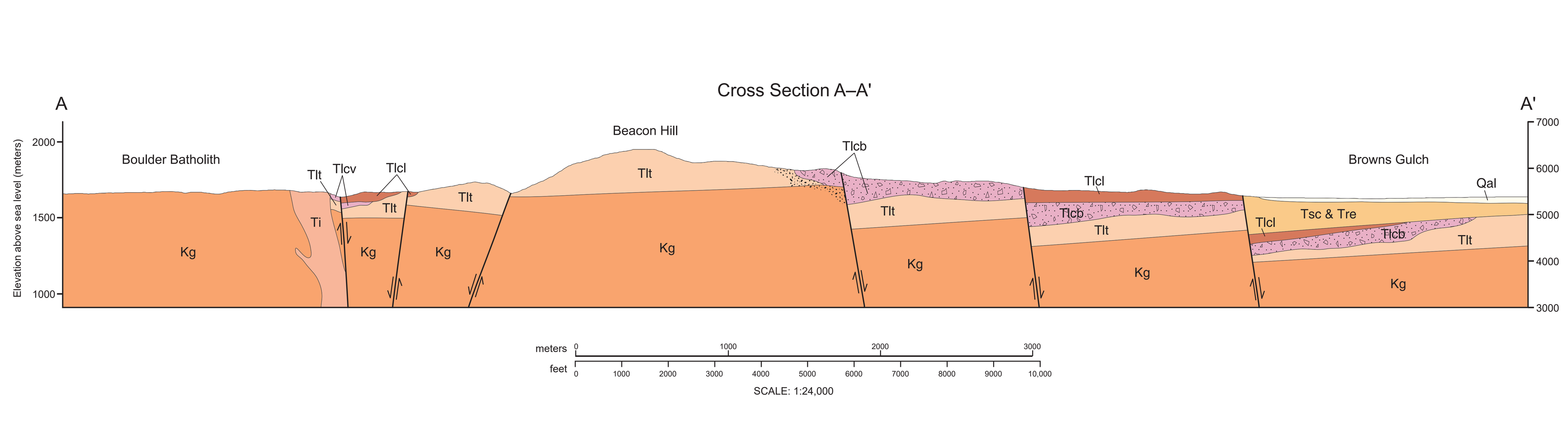

Research supported by the U.S. Geological Survey, National Cooperative Geologic Mapping Program, under USGS award number G13AC00210.
GIS production: Yiwen Li and Paul Thale, MBMG. Map layout: Susan Smith, MBMG. Editing: Susan Barth, MBMG.

CORRELATION DIAGRAM

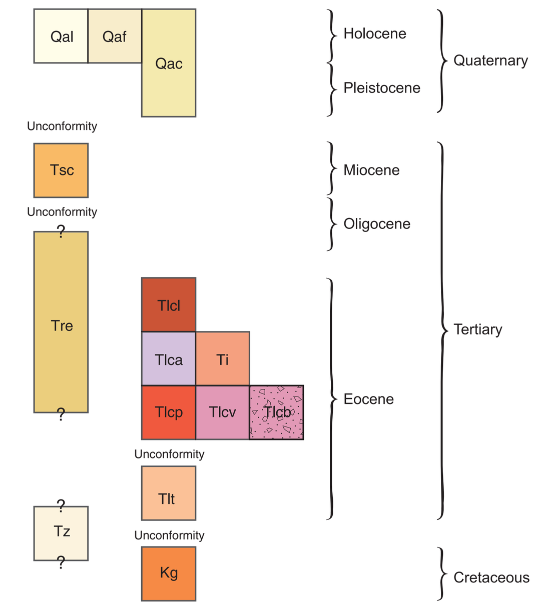

MAP SYMBOLS

Contact: dashed where uncertain; dotted where concealed

Normal fault: dashed where uncertain; dotted where concealed; tick shows fault plane dip value and direction; bar and ball on downthrown side

Strike-slip fault: dashed where uncertain; dotted where concealed; arrows show relative motion of blocks on either side of the fault

Strike and dip of inclined bedding

Strike and dip of inclined compaction foliation

Strike and dip of vertically oriented compaction foliation

Strike and dip of inclined flow bands

Strike and dip of vertically oriented flow bands

Strike and dip of inclined joint

Strike and dip of vertically oriented joint

KCS-13-104 Sample location showing sample number (please refer to table 1 for sample details)

Spring and direction of flow

Thermally fused margin

Abandoned or inaccessible vertical mine shaft at surface

INTRODUCTION

The Ramsay 7.5' quadrangle is located in Silver Bow County, between Butte and Anaconda in southwestern Montana (fig. 1). The I-90 corridor crosses the quadrangle at Ramsay (pop. 323), where topographic relief increases from southwest to northeast, from a minimum elevation of 5,275 ft (1,608 m) along Silver Bow Creek to a maximum elevation of 6,920 ft (2,109 m) in the hills southwest of Telegraph Gulch.

PREVIOUS MAPPING

Several geologic mapping studies have encompassed all, or part, of the Ramsay 7.5' quadrangle (fig. 1). Smedes (1968) and Derkey and Bartholomew (1988) mapped the quadrangle at 1:48,000 and 1:24,000 scale, respectively. A geologic map of the upper Clark Fork River Valley (Berg and Hargrave, 2004) includes the northwest corner of the quadrangle. A geologic map and hazards assessment of Silver Bow County (Elliott and McDonald, 2009) included a 1:48,000 map of the entire Ramsay 7.5' quadrangle. The Ramsay quadrangle was selected for updated geologic mapping to provide a modern interpretation of the volcanic deposits, and to obtain new geochemical and age data.

GEOLOGIC SUMMARY

Mineralization and uplift of the Boulder Batholith (Late Cretaceous–Eocene, between 79 and 58 Ma) occurred within a contractional (Laramide) setting that evolved into an extensional regime characterized by normal faulting by 53 Ma near Butte (Houston and Dilles, 2013). Eocene extension was accompanied by eruption of the 53 to 49 Ma Lowland Creek volcanic field (LCV) (Smedes, 1962; Smedes and Thomas, 1965; Dudas and others, 2010) ; (fig. 1).

LCV andesite–rhyolite (fig. 2; table 1) tuffs, lavas, and a conspicuous abundance of breccia forms a 2,624-ft (800-m)-thick sequence in the quadrangle. The LCV has a maximum regional thickness of 6,004 ft (1,830 m) (Smedes, 1962) and is primarily the product of caldera cycle volcanism (Foster, 1987). In the Ramsay 7.5' quadrangle, the LCV occurs as a 6.2-mi (10-km)-wide, northeast-trending band within the Boulder Batholith that covers over 309 mi^2 (800 km^2). Three discrete pulses of volcanic activity are recognized:

1. Caldera-forming rhyolite eruptions, equivalent to the "lower tuff" unit of Smedes (1962), produced at least one regionally extensive ignimbrite (Tlt) that erupted at 52.9 ± 0.14 Ma (Dudas and others, 2010); a less extensive, "upper tuff" unit erupted at 51.8 ± 0.14 Ma (Dudas and others, 2010). Upper tuff aged vent complexes occur near Butte (Houston and Dilles, 2013) and north of Boulder (Olson and others, 2017) ; (fig. 1). In the Ramsay 7.5' quadrangle, it is unclear if the mapped rhyolite ignimbrite (Tlt) consists of the "upper tuff," the "lower tuff," or both units, because of striking similarities in appearance and composition (Dudas and others, 2010). The "upper" and "lower" tuffs were not recognized in the present study.

2. Post-caldera fissure eruptions of rhyodacite porphyry lavas (Tlcp) between 51.8 and 50.0 Ma (Dudas and others, 2010; Scarberry and Elliott, 2016) filled northeast-trending basins. Several northeast-aligned vents occur in the adjacent Opportunity 7.5' quadrangle to the west, which may be a source for the porphyry lavas (Scarberry and Elliott, 2016). Previous workers have mistaken the rhyodacite sequence in the Ramsay 7.5' quadrangle as tuff (e.g., unit Trdp of Derkey and Bartholmew, 1988; Scarberry and others, 2015), and the sequence does exhibit contorted flow folding (fig. 3) that is similar to textures in rheomorphic ignimbrite (e.g., Andrews and Branney, 2011). However, an abundance of autoclastic breccia and vitrophyre at the margins of the rhyodacite porphyry is strong evidence that they are lavas, and not tuff. The lavas (Tlcp) are banked into footwall fault blocks that formed in the rhyolite ignimbrite (Tlt). Narrow bands of rhyolite breccia are densely welded, or "fused," locally where they are in contact with the younger porphyry lavas (Tlcp) (see map and cross-section). The rhyolite (Tlt) was fused by convection of superheated steam formed at the edges of the porphyry lavas (Tlcp) ; (e.g., Christiansen and Lipman, 1966). Vitrophyre (Tlcv) formed along quenched lava flow margins. Breccia (Tlcb) in vitrophyre and lavas formed as they dispersed through the landscape while cooling.

3. Resurgence of a local caldera floor between 51.1 and 50.0 Ma (Dudas and others, 2010; this study) was accompanied by rhyolite dikes (Ti) and related epithermal mineral deposits, and formation of the Hackney lava dome (Tlca). Resurgence led to lahar (Tlcl) formation on the flanks of the vent. A rhyolite dike (sample: KCS-13-100) cuts porphyry lava (Tlcp) and breccia (Tlcb) near the center of the quadrangle and has a high-precision TIMS U/Pb zircon age of 51.08 ± 0.02 Ma (table 2). Pillow lavas occur near the base of the lava dome; indicating that it encountered standing water. Field relationships in the Opportunity 7.5' quadrangle, to the west, show that the 50 Ma Hackney lava dome (Tlca) (Dudas and others, 2010) overlies and is younger than porphyry lavas (Tlcp), at least locally (Scarberry and Elliott, 2016).

STRUCTURAL GEOLOGY

The Lowland Creek volcanic field resembles the products of "graben volcanoes" (e.g., Aguirre-Diaz and others, 2008; Scarberry, 2017). Graben volcanoes form vents and fissures that align with the structural fabric of the tectonic basin that they are deposited in. LCV ignimbrites and lavas vented from northeast-trending fissures that mimicked northeast-striking "master" faults in the Boulder Batholith. Successive pulses of volcanism filled depressions in subsiding graben basins.

Topographic inversion of the LCV, whereby older tuffs are exposed at higher elevations than younger lavas, is supported by banking relationships between older and younger sequences. For example, the basal ignimbrite (Tlt) outcrops nearly 1,000 ft (305 m) higher in elevation than the Hackney lava dome (Tlca) in the southwest corner of the map. Porphyry lavas (Tlcp), vitrophyre (Tlcv), and breccia (Tlcb) are banked into the basal ignimbrite (Tlt) throughout the Ramsay 7.5' quadrangle, a relationship that implies at least 656 ft (200 m) of paleotopography prior to eruption of the porphyry lavas. Using the same logic, at least 394 ft (120 m) of paleotopography existed after rhyodacite volcanism, and before emplacement of the Hackney lava dome.

Most fault-related strain coincided with Eocene volcanism. The LCV is tilted 20–30° to the west–northwest in the quadrangle, consistent with moderate (10–0°) syn-volcanic tilt of the LCV near Butte (Houston and Dilles, 2013). Tertiary sediments (Tre, Tsc) are offset by about 49 ft (15 m) adjacent to the LCV in the southeastern part of the map.

Gravity data suggest that the Miocene–Oligocene valley fill may be as thick as 3,937 ft (1,200 m) in the southeastern corner of the map (Elliott and McDonald, 2009). Valley-fill deposits occur primarily as terrace sediments adjacent to Quaternary alluvial channels. These sediments consist of poorly indurated and stratified beds of cobble and pebble conglomerate and pale orange sand and silt (e.g., Berg and Hargrave, 2004). Two discrete sequences of sediments are recognized in the quadrangle: (1) Miocene–Oligocene clastic basin-fill sediments, and (2) Eocene low-energy, lake bed type deposits that record water saturation during the waning stages of Eocene volcanism. Valley-fill deposits occur primarily as terrace sediments adjacent to Quaternary alluvial channels. These sediments consist of poorly indurated and stratified beds of cobble and pebble conglomerate and pale orange sand and silt (e.g., Berg and Hargrave, 2004).

ECONOMIC GEOLOGY

Precious metal deposits occur at the Butte and Zenith Mine located in the southeast corner of the map, and the Tuxedo Mine located in the northwest corner of the map, near the contact between the LCV and the Boulder Batholith. The following descriptions are summarized from mining documents stored at the Montana Bureau of Mines and Geology in Butte (M. Delaney, written commun.).

The Butte and Zenith Mine occurs in the Boulder Batholith. Here, similar to conditions in Butte, the granite is cut by silver-bearing quartz veins and younger copper ores (summary in Houston and Dilles, 2013). A shaft, sunk in 1912, extended to 500 ft (152 m) depth with a cross cut at 460 ft (140 m). The shaft had been deepened to 1,031ft (314 m) when W.H. Weed examined the property in 1917. The shaft was extended an additional 500 ft (152 m) after 1922, but ore values were uneconomical and the property was left idle. As of this writing, a 10-ft (3-m)-high chain-link fence surrounds the mineshaft, which lies on private property.

Rhyolite breccia (Ti) hosts an ore deposit at the Tuxedo mine. Precious metal ores likely formed between 51.1 and 50.0 Ma during epithermal fluid circulation adjacent to the Late Cretaceous Boulder Batholith. Several generations of quartz are signs of crack-and-seal cycles related to caldera resurgence. The primary ore is silver-rich silicified hydrothermal breccia. The breccia is characterized by angular quartz vein clasts that are re-cemented in a microcrystalline, blue-gray quartz matrix. Precious metal occurrences include native gold, ruby silver (proustite and pyargyrite), and argentite. The Tuxedo mine operated intermittently from 1920 and into the 1950s when it consisted of a 100 ft (30 m) shaft and headframe intersected by two adits (now caved). The "Porter Tunnel," an adit driven into the hillside below the level of the shaft, yielded gold grades of up to 6 oz/ton. The property was of interest to mineral exploration companies as recently as the 1980s.

Table 1. Major oxide and trace element geochemical data. Major oxides normailized to 100 percent anhydrous.

Sample ID	KCS-13-104	KCS-13-90	KCS-13-55	KCS-13-59	KCS-13-105	KCS-13-86	KCS-13-52#	KCS-13-63	KCS-13-58	KCS-13-62	KCS-13-52	KCS-13-97	KCS-13-95	KCS-13-100	KCS-13-103
Map Unit	Tlt	Tlt	Tlt	Tlt	Tlt	Tlt	Tlcp	Tlcv	Tlcv	Tlcv	Tlcp	Tlt	Tlcv	Ti	Tlca
Lat	46.01824	46.05260	46.11133	46.10036	46.01292	46.03030	46.12350	46.10271	46.11941	46.09067	46.12284	46.04192	46.03526	46.04545	46.02180
Long	-112.75096	-112.64037	-112.64425	-112.63442	-112.74387	-112.66019	-112.63789	-112.69122	-112.66928	-112.64260	-112.64181	-112.70344	-112.70202	-112.67519	-112.74178
XRF (wt. %)															
SiO^2	71.15	72.70	72.92	72.50	70.09	71.23	70.56	65.59	69.63	64.96	70.73	73.30	69.39	72.15	61.60
TiO^2	0.41	0.31	0.30	0.35	0.37	0.37	0.35	0.53	0.48	0.52	0.34	0.29	0.50	0.37	0.90
Al^2O^3	15.10	14.54	14.62	15.01	15.47	15.19	15.64	16.18	15.75	16.04	15.72	14.54	14.99	14.59	16.09
$*FeO^T$	2.65	1.57	1.26	1.59	2.08	2.05	2.23	3.48	2.29	3.86	1.89	1.53	3.51	2.06	6.23
MnO	0.02	0.02	0.03	0.01	0.03	0.02	0.02	0.05	0.04	0.07	0.02	0.01	0.03	0.02	0.07
MgO	1.11	0.75	0.66	0.77	1.04	0.71	0.89	2.81	0.90	3.73	0.90	0.73	1.38	0.67	3.61
CaO	2.91	1.82	1.88	1.77	2.25	1.96	2.28	4.18	2.50	4.29	2.41	2.03	3.47	2.11	5.26
Na^2O	3.63	3.97	3.78	3.82	3.75	3.98	4.22	4.03	3.73	3.90	4.29	3.94	3.72	4.00	3.53
K^2O	2.91	4.24	4.41	4.06	4.79	4.37	3.69	3.00	4.46	2.50	3.58	3.56	2.88	3.92	2.51
P^2O^5	0.12	0.09	0.14	0.11	0.11	0.11	0.12	0.14	0.22	0.13	0.11	0.07	0.13	0.12	0.20
LOI	2.66	0.62	0.74	1.45	2.06	1.04	1.08	1.56	2.64	2.45	1.10	1.14	2.84	1.65	1.95
a.t.	97.04	99.04	98.56	97.39	96.95	98.19	97.95	98.03	96.11	97.14	98.21	98.64	95.74	98.12	97.52
Trace elements (ppm) (XRF)															
Ni	28	7	4	8	15	6	15	39	3	61	13	10	81	14	73
Cr	67	19	7	23	32	21	30	93	7	123	33	22	156	32	108
Sc	7	3	4	3	4	3	4	9	5	9	5	3	10	6	11
V	38	23	21	28	33	29	29	65	37	64	30	28	50	25	91
Ba	932	1102	1073	1146	1326	1189	1232	1144	2180	1014	1221	1161	935	1017	1026
Rb	74	160	198	148	145	160	108	84	121	84	104	112	79	164	63
Sr	632	386	423	396	505	419	569	677	756	646	612	576	549	386	598
Zr	119	151	149	168	193	192	140	149	184	141	140	124	127	179	181
Y	9	7	11	8	8	10	8	11	10	11	7	9	11	7	23
Nb	7	12	12	14	19	12	9	8	10	8	10	8	8	18	11
Ga	19	23	19	22	22	23	23	21	19	20	22	20	19	21	20
Cu	11	8	6	5	5	6	8	16	5	7	8	7	19	12	35
Zn	65	58	45	43	59	65	57	61	65	63	50	45	60	70	99
Pb	18	28	32	25	28	25	28	20	24	21	28	24	19	29	13
La	23	40	47	44	54	58	36	26	55	25	29	31	25	43	55
Ce	38	63	76	73	85	79	60	48	103	46	49	47	43	70	75
Th	6	19	23	21	24	23	11	7	17	7	11	10	7	22	9
Nd	19	21	30	25	29	33	22	18	38	17	18	19	20	24	40
U	1	5	9	5	4	4	3	3	4	3	3	2	4	4	2

*All Fe expressed as Fe^{2+}. All analyses performed by the Geoanalytical Laboratory at Washington State University.

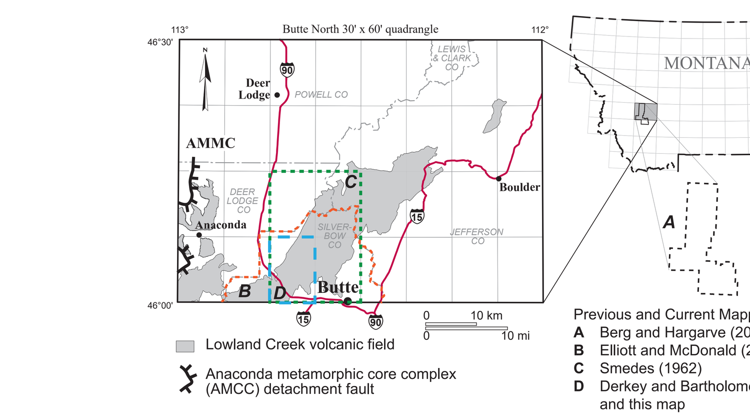

Figure 1. Location map (blue dashed line) and previous and current mapping in the Ramsay 7.5' quadrangle. Geology after Vuke and others, 2007.

DESCRIPTION OF MAP UNITS

M **Modified (Holocene)**—Land that has been modified during modern and active mine-waste reclamation efforts.

Sediments

Qal **Alluvium (Holocene)**—Well-sorted gravel, sand, silt, and clay in modern streams and floodplains. The unit is typically less than 33 ft (10 m) thick. Derkey and Bartholmew (1988) described two older alluvial surfaces that occur 3–6 ft (1–2 m) and 6–13 ft (2–4 m) above the modern floodplain. Thickness undetermined.

Qaf **Alluvial fan (Holocene)**—Fan-shaped, gently sloping masses of alluvium deposited at the mouths of constricted mountain stream channels. Thickness undetermined.

Qac **Colluvium (Holocene to Pliocene)**—Broad areas of debris found on hillsides and upland basins or parks. Consists of a mantle of stony soils and unconsolidated deposits of boulder debris, resulting from slope wash, mud flows, creep, and related mass-wasting processes. May include rock falls and alluvial fan deposits. Thickness less than 9 ft (3 m).

Tsc **Sixmile Creek Formation, undivided (Miocene)**—Pink to orange fine-grained ashy sediments characterized by floating quartz and feldspar grains supported in a fine-grained matrix. The formation contains a basal conglomerate that marks the unconformity with the underlying Renova Formation (Tre). Renova-aged paleosols occur as rip-ups in the unit.

Tre **Renova Formation, undivided (Eocene, Oligocene, and early Miocene)**—Pale yellow to tan and gray, fine-grained, massive to weakly fissile ashy mud that contains mammalian and plant fossils (Rasmussen, 1977).

Tz **Zenith Mine sediments (Miocene?–Eocene)**—Brick red, silicified to poorly indurated and oxidized, fine-grained sediment and weathered Eocene volcanic rocks. Mapped as rhyolite by Derkey and Bartholomew (1988) and as red volcanogenic pebbly clay and silt, or altered andesite (Elliott and McDonald, 2009 and references therein). The presence of Eocene volcanic rocks in the deposit indicates that the unit formed concurrent with, or after, the LCV. Good exposure occurs along the west and southwest sides of the Butte and Zenith mine where red clays mantle Late Cretaceous granite, aplite, and quartz veins. Exposure of the sequence occurs primarily adjacent to a block of Late Cretaceous granite that hosts the Butte and Zenith mine. Here the unit may have been produced by grinding, oxidation, and fluid alteration within a fault zone. The red and oxidized sediments may also have formed when porphyry lavas erupted onto paleosols formed in the lower tuff (Tlt). Elliott and McDonald (2009) interpreted these sediments as 492 ft (150 m) thick and proposed a Miocene–Oligocene age.

The Lowland Creek Volcanic Field (Eocene)

Tlcl **Lahars**—Heterolithologic, matrix-supported, and generally poorly indurated debris flow deposits produced by landslides or mudflows of pyroclastic material on the flanks of a volcano. The lahar deposits consist of sub-angular to sub-rounded, poorly sorted igneous clasts including rhyodacite porphyry lavas (Tlcp) and vitrophyre (Tlcv), rhyolite ignimbrite (Tlt), and breccia (Tlcb). These clasts are encased in loosely cemented lapilli and mud. Lahar deposits are widespread at topographic elevations below approximately 5,000 ft (1,524 m) in the south-central part of the quadrangle, between Beacon Hill and Chinamans Spring. The deposits are semi-indurated at higher elevations and labile and reworked by fluvial processes at lower elevations. Thickness undetermined.

Tlca **Andesite–dacite Hackney lava dome complex**—Black, glassy, crystal-poor to aphanitic lava, agglutinate, and phreatomagmatic deposits. Composition ranges from andesite–dacite (SiO_2 = 60.0–63.0 wt. percent; fig. 2, table 1) ; (Derkey and Bartholomew, 1988; Dudas and others, 2010; Scarberry and Elliott, 2016) that form the capping sequence of the LCV. Includes aphanitic and porphyritic dacite breccia (units Tda and Tdp, respectively, of Derkey and Bartholomew, 1988). Dudas and others (2010) refer to the sequence as the upper lava dacite and report $^{40}Ar/^{39}Ar$ eruption ages of 49.33 ± 0.34 Ma (plateau) and 50.47 ± 1.02 Ma (total gas) from plagioclase. Subvolcanic exposure of the sequence is suggested by platy outcrops that exhibit subhorizontal and subvertical flow bands. Subaerial deposits of the unit are vesicular and contain autobrecciated flow bases and pillow lavas locally (see also Scarberry and others, 2015). The exposed thickness is approximately 328 ft (100 m).

Ti **Rhyolite intrusive rocks, related breccia, and zones of hydrothermal alteration**—Gray resistant and platy, porphyritic dike rocks. Zones of intense hydrothermal alteration occur within and adjacent to intrusions. Alteration zones are recognized by white to tan, intensely bleached and silicified coarsely porphyritic rocks. The unit includes precious-metal ores, rhyolite breccia, and silica veins at the Tuxedo Mine. Zones of argillic to mildly propylitic alteration occur locally. A northeast-trending rhyolite (SiO_2 = 72.2 wt. percent; fig. 2, table 1) dike exposed continuously for approximately 3,280 ft (1,000 m) near the center of the quadrangle (KCS-13-100) has a U/Pb zircon age of 51.084 ± 0.023 Ma (table 2). The dike contains glass, biotite, quartz, hornblende, 1- to 2-cm-long granite xenoliths, and 1-cm-long zoned plagioclase xenocrysts. Resorption textures in the dike rock are evident in hand specimens.

Tlcp **Rhyodacite lava flows**—Dark gray to gray and maroon, coarsely porphyritic, rhyodacite (SiO_2 = 67.0–71.9 wt. percent; fig. 2, table 1) (Derkey and Bartholomew, 1988; Dudas and others, 2010; Scarberry and Elliott, 2016). The lavas are platy, crystal-poor (10–15 percent), and exhibit near-planar flow bands, with similarly oriented lithophysal laminations, at the base of the sequence. The lavas are crystal-rich porphyry with highly contorted flow banding (fig. 3) in the upper parts of individual lava flows. Plagioclase crystals commonly larger than 5 mm wide, biotite, hornblende, and quartz are the primary phenocrysts in a devitrified and oxidized groundmass. $^{40}Ar/^{39}Ar$ ages of 51.79 ± 0.51 Ma (Scarberry and Elliott, 2016) and 51.79 ± 0.07 Ma (Dudas and others, 2010) are reported for the unit. 52.87 ± 0.26 Ma clasts of similar composition are observed in tuff of the basal ignimbrite (Tlt) near Anaconda ($^{40}Ar/^{39}Ar$; Dudas and others, 2010). The sequence is up to 1,148 ft (350 m) thick in the quadrangle.

Tlcv **Rhyodacite vitrophyre**—Black and vitric lava that contains abundant plagioclase phenocrysts and occasional biotite. Exposed at, or near, the base of the porphyry lava sequence (Tlcp) and is a facies of the same volcanic pulse. Derkey and Bartholomew (1988) mapped the unit as rhyodacite welded tuff (their unit Trdp). A biotite-rich sample (KCS-13-62) collected south of Meadow Gulch in the northwest part of the quadrangle is dacite (fig. 2, table 1). In the Meadow Gulch area, the vitrophyre is associated with a fault and/or a rhyolite intrusion and may be unrelated to the rhyodacite porphyry lavas. Exposures of the unit are typically < 32 to 65 ft (10 to 20 m) thick. The vitrophyre is over 328 ft (100 m) thick where it is brecciated and banked into rhyolite ignimbrite (Tlt) north of Ramsay.

Tlcb **Breccia**—Predominately autoclastic flow breccia that formed during emplacement of rhyodacite porphyry lavas (Tlcp) and vitrophyre (Tlcv). Autoclastic flow breccia is generally monolithologic, matrix- and clast-supported, and variably indurated. Autoclastic flow breccia occurs at both the top and base of the porphyry lavas (Tlcp) and vitrophyre (Tlcv). Excellent outcrops of the basal breccia occur in the Opportunity 7.5' quadrangle (Scarberry and Elliott, 2016), where it is recognized by white to salmon pink, poorly indurated and matrix-supported block and ash deposits that transition up section to massive, clast-supported, autoclastic breccia. Autoclastic breccia associated with the top of the rhyodacite lavas (Tlcp) is recognized by flow-banded blocks of rhyodacite in a lava matrix. Breccia in vitrophyre is dark, glassy, and monolithologic. Rapid cooling at the margins of the porphyry lavas (Tlcp) formed vitrophyre (Tlcv), which turned to breccia in locations where the chilled margin of the flow continued to spread. Excellent outcrops of this unit occur north of Ramsay, and adjacent to the "fused" contact with rhyolite ignimbrite (Tlt) (see map and cross section). The unit also includes small volumes of monolithic clast-supported and intensely silicified fissure breccia of the Hackney lava dome complex (see also Scarberry and others, 2015).

Tlt **Rhyolitic ignimbrite**—White and gray, lithic- and crystal-rich and variably welded tuff. Three distinct horizons are recognized and are gradational to one another. The bottom 262 ft (80 m) consists of non-welded, pumice- and lithic- and biotite-rich dacite–rhyolite (SiO_2 = 66.0–70.4 wt. percent; fig. 2, table 1) tuff that ranges in age from 53.36 ± 0.13 to 52.64 ± 0.39 Ma ($^{40}Ar/^{39}Ar$; Derkey and Bartholomew, 1988; Dudas and others, 2010; Scarberry and Elliott, 2016). The base of the section is exposed north of Telegraph Gulch in the northeastern corner of the map. Here, silicified pebble-sand conglomerate is cut by chalcedony veins that transition up section to non-welded lithic-rich tuff. The overlying 492 ft (150 m) of the section is non-welded air-fall and base surge deposits that have sparse, thin, laminar and densely welded tuff interbeds. Surge deposits are best exposed south of Telegraph Gulch (KCS-13-55), where they overlie lithic-bearing ash beds. The uppermost 229 ft (70 m) of the section consists of moderately welded rhyolite tuff (SiO_2 = 70.4–75.1 wt. percent; fig. 2, table 1) with a $^{40}Ar/^{39}Ar$ age of 52.50 ± 0.32 (Scarberry and Elliott, 2016). Moderately welded tuff has a compaction foliation defined by compressed pumice. Gas escape voids that formed during vapor-phase crystallization in poorly welded tuff outcrops are also flattened. Good exposures occur south of Telegraph Gulch (KCS-13-59), throughout the east–central part of the quadrangle (KCS-13-90), and within the southeastern corner of the quadrangle (KCS-13-86). A biotite-rich vitrophyre exposed north of Silver Bow Creek (KCS-13-105) in the southwest corner of the map is like the middle section of the unit elsewhere but differs in that it transitions to a mildly porphyritic rheomorphic tuff, rather than the laminar, coarsely porphyritic tuff observed elsewhere. In total, the sequence is over 984 ft (300 m) thick in the quadrangle.

The Boulder Batholith (Late Cretaceous)

The Boulder Batholith consists of about 15 plutons exposed over 1,737 mi^2 (4,500 km^2) in southwestern Montana, and hosts a world-class ore deposit at Butte (summary in Houston and Dilles, 2013; Czehura, 2006). The batholith is largely zoned in terms of age and composition (Tilling and others, 1968; Klepper and others, 1971; du Bray and others, 2012). Granodiorite to gabbro plutons along the north, east, and southern margins of the batholith crystallized between about 81 and 76 Ma, while the principal body, the Butte pluton, formed between about 75 and 74 Ma (Lund and others, 2002; Berger and others, 2011).

Kg **Granitic rocks, undivided (Late Cretaceous)**—Most of the unit is granitic rock of the Butte pluton and smaller volumes of alaskite, aplite, pegmatite, monzonite, and granodiorite. Smedes (1968) described three groups of Boulder Batholith rocks within the quadrangle: (1) light-colored, sheet-like, and irregular masses of alaskite, aplite, and pegmatite, the distribution of which remains largely unmapped; (2) light-colored, coarse-grained quartz monzonite and granodiorite of the Butte pluton. U/Pb zircon ages for the Butte granite are 74.5 ± 0.9 Ma (Lund and others, 2002) and 76.28 ± 0.14 Ma (Martin and others, 1999); and (3) medium to dark granodiorite containing 3–5 percent biotite and 1 percent opaque minerals.

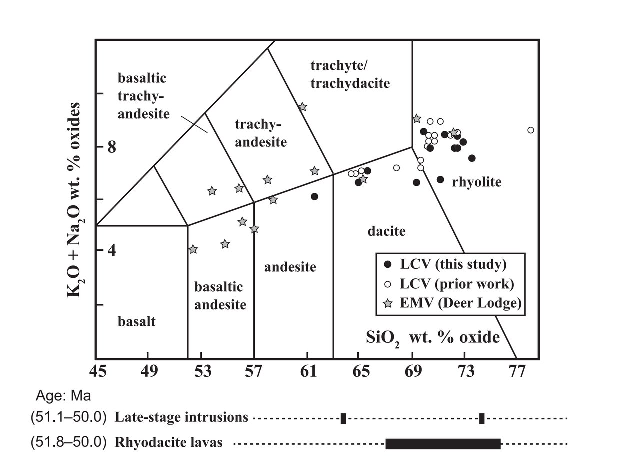

Figure 2. Volcanic rock types diagram after Le Bas and others (1986). Source of data: LCV (prior work) is from Derkey and Bartholomew (1988) and Dudas and others (2010), and EMV (Deer Lodge) is from Scarberry (2016). The bottom of the figure shows the duration and compositional range for pulses of activity in the Lowland Creek volcanic field.

Figure 3. Flow-banded rhyodacite porphyry lavas (Tlcp) in the Lowland Creek volcanic field.

Table 2. CA-IDTIMS U-Pb isotopic data.

Grain (a)	Th/U (b)	$^{206}Pb^*$ x10^{-13} mol (c)	mol % $^{206}Pb^*$ (c)	Pb^*/Pbc (c)	Pbc (pg) (c)	$^{206}Pb/^{204}Pb$ (d)	$^{208}Pb/^{206}Pb$ (e)	Radiogenic Isotopic Ratios: $^{207}Pb/^{206}Pb$ (e)	% err (f)	$^{207}Pb/^{235}U$ (e)	% err (f)	$^{206}Pb/^{238}U$ (e)	% err (f)	corr. coef.	Radiogenic Isotopic Dates: $^{207}Pb/^{206}Pb$ (g)	± (f)	$^{207}Pb/^{235}U$ (g)	± (f)	$^{206}Pb/^{238}U$ (g)	± (f)
KCS-13-100																				
z3	0.517	0.7539	99.54%	66	0.29	3958	0.166	0.047272	0.178	0.052104	0.227	0.007994	0.074	0.762	63.0	4.2	51.57	0.11	51.329	0.03
z2	0.560	0.3433	99.15%	36	0.24	2128	0.180	0.047243	0.357	0.052032	0.407	0.007988	0.081	0.689	61.5	8.5	51.50	0.20	51.289	0.04
z6	0.479	0.6688	99.54%	64	0.26	3891	0.154	0.047160	0.181	0.051926	0.231	0.007986	0.073	0.761	57.3	4.3	51.40	0.12	51.275	0.03
z1	0.624	0.5202	99.12%	35	0.38	2048	0.200	0.047138	0.254	0.051725	0.303	0.007958	0.076	0.722	56.2	6.1	51.21	0.15	**51.100**	**0.03**
z4	0.512	0.4836	99.36%	47	0.26	2840	0.164	0.047167	0.227	0.051717	0.278	0.007952	0.081	0.719	57.7	5.4	51.20	0.14	**51.062**	**0.04**
z5	0.503	0.4740	99.68%	92	0.13	5554	0.161	0.047158	0.163	0.051734	0.217	0.007956	0.074	0.809	57.3	3.9	51.22	0.11	**51.087**	**0.03**

Notes:
(a) z1, z2, etc. are labels for single zircon grains or fragments chemically abraded at 180°C for 12 h; dates in bold used in the weighted mean calculation.
(b) Model Th/U ratio calculated from radiogenic $^{208}Pb/^{206}Pb$ ratio and $^{207}Pb/^{235}U$ date.
(c) Pb* and Pbc are radiogenic and common Pb, respectively. mol % $^{206}Pb^*$ is with respect to radiogenic and blank Pb.
(d) Measured ratio corrected for spike and fractionation only. Samples were spiked with the ET535 tracer, and use an external Pb fractionation correction of 0.20 ± 0.02 (1-sigma) %/amu (atomic mass unit), based on analysis of NBS-981 and NBS-982.
(e) Corrected for fractionation, spike, common Pb, and initial disequilibrium in $^{230}Th/^{238}U$. All common Pb was assigned to procedural blank with a composition of $^{206}Pb/^{204}Pb$ = 18.042 ± 0.61%; $^{207}Pb/^{204}Pb$ = 15.537 ± 0.52%; $^{208}Pb/^{204}Pb$ = 37.686 ± 0.63% (1-sigma).
(f) Errors are 2-sigma, propagated using algorithms of Schmitz and Schoene (2007).
(g) Calculations based on the decay constants of Jaffey and others (1971). $^{206}Pb/^{238}U$ and $^{207}Pb/^{206}Pb$ ratios and dates corrected for initial disequilibrium in $^{230}Th/^{238}U$ using Th/U [magma] = 3.

ANALYTICAL SUMMARY

Bulk Geochemistry

Bulk composition data for 15 rocks collected in the Ramsay 7.5' quadrangle is reported in table 1. Rock samples were analyzed by technicians at the Peter Hooper GeoAnalytical Lab at Washington State University using the X-Ray fluorescence methods described by Johnson and others (1999).

U-Pb Geochronology

LA-ICPMS

Abundant populations of equant to prismatic zircon crystals were separated from sample KCS-13-100 by technicians at Boise State University using conventional density and magnetic methods. The entire zircon separate was placed in a muffle furnace at 900°C for 60 h in quartz beakers to anneal minor radiation damage; annealing enhances cathodoluminescence (CL) emission, promotes more reproducible interelement fractionation during laser ablation inductively coupled plasma mass spectrometry (LA-ICPMS), and prepares the crystals for subsequent chemical abrasion (Mattinson, 2005). Following annealing, individual grains were hand-picked and mounted, polished and imaged by CL on a scanning electron microscope.

CL imaging of the zircons extracted from KCS-13-100 revealed predominantly weakly luminescent, oscillatory-zoned crystals, with a minority containing highly luminescent cores with irregular non-luminescent rims. LA-ICPMS analysis confirmed the high U content and Eocene age of the low-luminescence zircons. Several luminescent crystal cores were identified as Archean to Proterozoic in age; others yielded Cretaceous ages. Twenty-one spot analyses were rejected as biased by inherited cores and a single anomalously young analysis was also rejected. The remaining 42 spot analyses yielded a normal distribution with a weighted mean $^{206}Pb/^{238}U$ date of 50.4 ± 0.4 (1.1) Ma (MSWD = 1.4).

CA-IDTIMS

Following CL imaging and LA-ICPMS analysis, selected zircon crystals were extracted from the epoxy mount and analyzed by chemical abrasion ID-TIMS analysis for a more precise and accurate age of crystallization. Grains plucked from the grain mount were selected on the basis of their oscillatory zonation, low CL emission, high U content, and Eocene apparent ages by LA-ICPMS.

Three of six crystals analyzed by this method (table 2) yielded older ages of 51.28 to 51.33 Ma. These ages are likely biased by subtle inherited cores, recalling that more obvious inheritance is observable in CL imagery. The other three crystals yielded equivalent isotope ratios with a weighted mean $^{206}Pb/^{238}U$ date of 51.084 ± 0.023 (0.034) [0.065] Ma (MSWD = 0.95; probability of fit = 0.3886). This is interpreted as the emplacement and crystallization age of the intrusive. The $^{206}Pb/^{238}U$ date is slightly older, but it is within the error of that produced by LA-ICPMS (50.4 ± 1.1 Ma) and has a much greater precision than LA-ICPMS. Greater accuracy is also attributed to the $^{206}Pb/^{238}U$ date of 51.084 ± 0.023 because chemical abrasion removes Pb-loss domains that cause a bias to younger ages in LA-ICPMS results.

REFERENCES

Aguirre-Diaz, G.J., Labarthe-Hernandez, G., Tristan-Gonzalez, M., Nieto-Obregon, J., and Guiterrez-Palomares, I., 2008, Chapter 4: The ignimbrite flare-up and graben calderas of the Sierra Madre Occidental, Mexico, *in* Developments in volcanology-caldera volcanism: Analysis, modelling and response, v. 10, p. 143–180.
Andrews, G.D.M., and Branney, M.J., 2011, Emplacement and rheomorphic deformation of a large, lava-like rhyolitic ignimbrite: Gray's Landing, southern Idaho: Geologic Society of America Bulletin, v. 123, p. 725–743.
Berg, R.B., and Hargrave, P.A., 2004, Geologic map of the Upper Clark Fork Valley: Montana Bureau of Mines and Geology Open-File Report 506, 1:50,000 scale.
Berger, B.R., Hildenbrand, T.G., and O'Neill, J.M., 2011, Control of Precambrian basement deformation zones on emplacement of the Laramide Boulder batholith and Butte mining district, Montana, United States: U.S. Geological Survey Scientific Investigations Report 2011-5016, 29 p.
Christiansen, R.L., and Lipman, P.W., 1966, Emplacement and thermal history of a rhyolite lava flow near Fortymile Canyon, southern Nevada, Geological Society of America Bulletin, v. 77, p. 671–684.
Czehura, S., 2006, Butte: A world class ore deposit: Mining Engineering, v. 58, p. 14–19.
Derkey, P.D., and Bartholomew, M.J., 1988, Geologic map of the Ramsay quadrangle, Montana: Montana Bureau of Mines and Geology Geologic Map 47.
du Bray, E.A., Aleinikoff, J.N., and Lund, K., 2012, Synthesis of petrographic, geochemical, and isotopic data for the Boulder Batholith, southwest Montana: U.S. Geological Survey Professional Paper 1793, 39 p.
Dudas, F.O., Ispolatov, V.O., Harlan, S.S., and Snee, L.W., 2010, $^{40}Ar/^{39}Ar$ geochronology and geochemical reconnaissance of the Eocene Lowland Creek volcanic field, west-central Montana: Journal of Geology, v. 118, no. 3, p. 295–304.
Elliott, C.G., and McDonald, Catherine, 2009, Geologic map and geohazard assessment of Silver Bow County, Montana: Montana Bureau of Mines and Geology Open-File Report 585; 1:50,000 scale.
Foster, F., 1987, Epithermal precious-metal systems associated with an Eocene cauldron: Lowland Creek volcanic field, southwestern Montana, *in* Berg, R.B., and Breuninger, R.H., eds., Guidebook of the Helena area, west-central Montana: Montana Bureau of Mines and Geology Special Publication 95, p. 53–54.
Houston, R.A., and Dilles, J.H., 2013, Structural geologic evolution of the Butte District, Montana: Economic Geology, v. 108, p. 1397–1424.
Klepper, M.R., Ruppel, E.T., Freeman, V.L., and Weeks, R.A., 1971, Geology and mineral deposits, east flank of the Elkhorn Mountains, Broadwater County, Montana: U.S. Geological Survey Professional Paper 665, 1:48,000 scale.
Jaffey, A.H., Flynn, K.F., Glendenin, L.E., Bentley, W.C., and Essling, A.M., 1971, Precision measurements of half-lives and specific activities of ^{235}U and ^{238}U, Physical Review C, v. 4, p. 1889–1906.
Johnson, D.M., Hooper, P.R., and Conrey, R.M., 1999, XRF analysis of rocks and minerals for major and trace elements on a single low dilution Li-tetraborate fused bead: JCPDS-International Centre for Diffraction Data, p. 843–867.
LeBas, M.J., LeMaitre, R.W., Streckeisen, A., and Zanettin, B., 1986, A chemical classification of volcanic rocks based on the total alkali silica diagram: Journal of Petrology, v. 27, p. 745–750.
Lund, K., Aleinikoff, J., Kunk, M., Unruh, D., Zeihen, G., Hodges, W., duBray, E., and O'Neill, J., 2002, SHRIMP U-Pb and $^{40}Ar/^{39}Ar$ age contrasts for relating plutonism and mineralization in the Boulder batholith region, Montana: Economic Geology, v. 97, p. 241–267.
Martin, M., Dilles, J., and Proffett, J.M, 1999, U-Pb geochronologic constraints for the Butte porphyry system [abs.]: Geological Society of America Abstracts with Programs, v. 31, no. 7, p. A380.
Mattinson, J.M., 2005, Zircon U-Pb chemical abrasion ("CA-TIMS") method: combined annealing and multi-step partial dissolution analysis for improved precision and accuracy of zircon ages: Chemical Geology, v. 220, p. 47–66.
Olson, N.H., Sepp, M.D., Dilles, J.H., Mankins, N.E., Blessing, J.M., and Scarberry, K.C., 2017, Geologic map of the Mount Thompson 7.5' quadrangle, southwest Montana: Montana Bureau of Mines and Geology EDMAP-11.
Rasmussen, D.L. 1977, Geology and mammalian paleontology of the Oligocene-Miocene Cabbage Patch Formation, central-western Montana: Univ. Kansas Ph.D. Dissertation, 794 p.
Scarberry, K.C., Korzeb, S.L., and Smith, M.G., 2015, Origin of Eocene volcanic rocks at the south end of the Deer Lodge Valley, Montana: Northwest Geology, v. 44, p. 201–212.
Scarberry, K.C., 2016, Geologic map of the Sugarloaf Mountain 7.5' quadrangle, Deer Lodge, Jefferson, and Powell Counties, MT: Montana Bureau of Mines and Geology Open-File Report 674.
Scarberry, K.C., and Elliott, C.G., 2016, Geologic map of the Opportunity 7.5' quadrangle, Deer Lodge and Silver Bow Counties, MT: Montana Bureau of Mines and Geology Open-File Report 683.
Scarberry, K.C., 2017, Eruption history and origin of precious metal ore deposits: The Eocene Lowland Creek Volcanic Field, southwestern Montana, *in* Korzeb, S.L. and Scarberry, K.C., Proceedings of the 2016 Mining and Mineral Symposium: Montana Bureau of Mines and Geology Open-File Report 685.
Smedes, H.W., 1968, Preliminary geologic map of part of the Butte North quadrangle, Silver Bow, Deer Lodge, and Jefferson Counties, Montana: U.S. Geological Survey Open-File Report 68-254, 1 sheet, 1:36,000.
Smedes, H.W., 1962, Lowland Creek volcanics, an Upper Oligocene formation near Butte, Montana: The Journal of Geology, v. 70, no. 2, p. 255–266.
Smedes, H.W., and Thomas, H.H., 1965, Reassignment of the Lowland Creek Volcanics to Eocene age: Journal of Geology, v. 73, no. 3, p. 508–510.
Schmitz, M.D., and Schoene, B., 2007, Derivation of isotope ratios, errors and error correlations for U-Pb geochronology using ^{205}Pb-^{235}U-(^{233}U)-spiked isotope dilution thermal ionization mass spectrometric data: Geochemistry, Geophysics, Geosystems (G3) 8, Q08006, doi:10.1029/2006GC00149.
Tilling, R.I., Klepper, M.R., and Obradovich, J.D., 1968, K-Ar ages and time span of emplacement of the Boulder batholith, Montana: American Journal of Science, v. 266, p. 671–689.
Vuke, S.M., Porter, K.W., Lonn, J.D., and Lopez, D.A., 2007, Geologic Map of Montana: Montana Bureau of Mines and Geology, Geologic Map 62, 73 p., 2 sheets, scale 1:500,000.

MBMG
Montana Bureau of Mines and Geology

Geologic Map 72

Geologic Map of the Ramsay 7.5' Quadrangle, Southwestern Montana

Mapped and compiled by Kaleb C. Scarberry

2019